Title

CO2 flow modeling in a coupled wellbore and aquifer system: Details of pressure, temperature, and dry-out

Authors

Zamani, Nematollah
Oldenburg, Curtis M
Solbakken, Jonas
et al.

Publication Date

2024-02-01

DOI

10.1016/j.ijggc.2024.104067

CO_2 Flow Modeling in a Coupled Wellbore and Aquifer System: Details of Pressure, Temperature, and Dry-Out

Nematollah Zamani [a*], Curtis M. Oldenburg[b], Jonas Solbakken [a], Morten G. Aarra [a], Patrick Kowollik[c], Hakan Alkan[d], Mohd Amro[d], Taofik Nassan[d], Jose K.P. Estrada[e], Oleksandr Burachok[c]

[a] NORCE Norwegian Research Centre., Bergen, Norway

[b] Energy Geosciences Division, Lawrence Berkeley National Laboratory, Berkeley, CA, United States

[c] Wintershall Dea AG, Germany

[d] Technical University Bergakademie Freiberg (TU-BAF), Germany

[e] Montanuniversität Leoben, Austria

* Corresponding author:

Nematollah Zamani

Nematollah.zamani@norceresearch.no

Nygårdsgaten 112, 5008 Bergen, Norway

Telephone: (+47) 56 10 71 50

Note: This is the manuscript form of the published paper which should be cited as:

Zamani, N., Oldenburg, C.M., Solbakken, J., Aarra, M.G., Kowollik, P., Alkan, H., Amro, M.M., Nassan, T.H., Estrada, J.K. and Burachok, O., 2024. CO2 flow modeling in a coupled wellbore and aquifer system: Details of pressure, temperature, and dry-out. *International Journal of Greenhouse Gas Control*, *132*, p.104067.

https://doi.org/10.1016/j.ijggc.2024.104067

Abstract:

In order to understand the details of thermal and hydrologic processes attending CO_2 injection into a deep aquifer in the context of Carbon Capture and Storage (CCS), we have carried out coupled well-reservoir simulations of CO_2 injection using the simulator T2WELL-ECO2M. We focus on the injection of cold, dry CO_2 into a warm aquifer and analyze in detail the thermal and hydraulic processes of the coupled well-reservoir system. The results demonstrate the effectiveness of T2WELL in accurately modeling non-isothermal, multiphase flow, phase changes, and identifying dry-out regions in porous media.

We simulated heat exchange with the ambient environment, friction effects, convection, exothermic dissolution in brine, and cooling due to both Joule-Thomson effect and water vaporization. The temperature profile within the wellbore deviated from the geothermal profile, impacting CO_2 properties at the bottomhole. The simulation revealed the presence of three fronts in the formation: the CO_2 saturation, thermal, and evaporation fronts. The thermal and evaporation fronts were located farther behind the saturation front, indicating limited dry-out and thermal effects near the wellbore.

This simulation capability and insights gained in this study form a foundation for ongoing work such as sensitivity analyses, injection optimization, performance assessment, and operational decision support.

Keywords: Coupled well-reservoir system, T2WELL-ECO2M, Thermal processes, Dry-out region, Injectivity

1. Introduction

Carbon Capture and Storage (CCS) is a practical approach to decreasing the concentration of CO_2 in the atmosphere and mitigating the greenhouse effect, as well as a transitional step towards renewable energy sources. (e.g., Vilarrasa & Rutqvist, 2017). CCS includes capturing CO_2 from industrial sources, transport to a storage site, and injection through the wellbore into specific geologic underground formations. The injection of CO_2 into subsurface formations is a well-established technology in the oil and gas industry, serving as an enhanced oil recovery method for several decades (Hill et al., 2013; Kumar et al., 2022). Despite relatively slow development of CCS worldwide, several pilot and commercial scales CO_2 storage projects have been or are being performed to prove the reliability and applicability of CO_2 injection and to reduce knowledge gaps in providing safe CCS technology (Alkan et al., 2023; Finley et al., 2013; Hovorka et al., 2006; Litynski et al., 2013; Mathieson et al., 2011; Movahedzadeh et al., 2021; Page et al., 2020; Preston et al., 2005; Rangriz Shokri et al., 2021; Sato et al., 2011; Torp & Gale, 2004; Würdemann et al., 2010). Nevertheless, significant CO_2 injection over an extended period for storage purposes may pose multiple challenges, including impairments to injectivity and potential leakage from the storage complex. These challenges may hinder the fast implementation of CCS projects (Kelemen et al., 2019).

Proper assessment of a CCS project requires accurately evaluating reservoir behavior in response to physical, chemical, and thermal perturbation induced by large-scale CO_2 injection over a long injection period (André et al., 2010). Thermophysical properties of pure CO_2, such as density, viscosity, enthalpy, and phase behavior, depend on pressure and temperature, and play a crucial role in CO_2 injectivity, storage capacity, and storage safety (Sokama-Neuyam et al., 2020, 2022, Buursink, 2014; Al-Khdheeawi et al., 2018). Due to significant variations in temperature and pressure profiles along the wellbore, thermophysical properties of CO_2 at the bottomhole are different from its properties at the wellhead (Henninges et al., 2011; Lindeberg, 2011; Lu & Connell, 2014b; Vilarrasa et al., 2013). Multiple processes can influence the temperature profile along the wellbore. Heat exchange through the casing walls during CO_2 flow in the wellbore through different geological formations is the primary source of temperature change. This heat exchange depends on flow rate, well completion and isolation status, geothermal gradient, and thermal properties of the surrounding formations (Vilarrasa et al., 2013). In addition, frictional loss, thermal conduction, convection, and the Joule-Thomson effect can alter temperature profiles (André et al., 2010; Vilarrasa & Rutqvist, 2017).

In addition, mutual interaction between the wellbore and storage formation, strong transient flow during CO_2 injection operation start-up and shut-in, phase transition along the wellbore, dominancy of inertia force within the wellbore, and possible leakage of fluid through casing and cement near the wellbore emphasize the importance of having a reliable simulation tool that can adequately describe CO_2 flow in the wellbore. Despite its importance for evaluating CO_2 storage, only a few papers have addressed CO_2 flow in the well (Liu et al., 2016; Lu & Connell, 2014b; Pan et al., 2011; Piao et al., 2018; Strpic et al., 2021). Most CO_2 injection simulation studies have focused on CO_2 flow in porous media, while the flow in the wellbore has either been disregarded (Dalkhaa et al., 2022; Kim et al., 2014) or coupling separate software for wellbore and reservoir simulation (Aakre et al., 2018), or treated as a part of porous media by assigning equivalent parameters (André et al., 2010). This latter approach is called the equivalent porous media approach (EPM). However, this approach overlooks the distinct nature of flow in porous media and the wellbore, which we will elaborate on further below.

As CCS gains attention as a viable solution for mitigating global warming, there is a growing need for reliable simulation tools to design and optimize CCS projects, particularly in the near-wellbore region. The success of CCS projects relies on the ability to predict the behavior of CO_2 in the near wellbore region, which is influenced by complex thermodynamic and fluid flow processes. One of the critical challenges in CCS projects is accurately modeling the behavior of CO_2 as it flows through the wellbore and storage formation. To address this challenge, we investigate the strength and limitations of T2WELL-ECO2M, a simulation code from the TOUGH family, for modeling non-isothermal flow in the wellbore and storage formation, focusing on answering critical industrial questions related to the injection of CO_2 into saline aquifers. Specifically, we aim to understand how T2WELL-ECO2M can be used to model the behavior of CO_2 during injection, including thermal effects, phase changes, multiphase flow, and the occurrence of the dry-out region in the near wellbore region. By doing so, we hope to provide insights into the capabilities and limitations of this simulation tool and the potential challenges and opportunities for designing and optimizing CO_2 storage projects. The finding of this study serves as the basis for ongoing research on parameter sensitivity analysis for CO_2 flow in the wellbore and reservoir to address some of the fundamental industrial challenges summarized as follows:

- Near-wellbore effect: Under what conditions does a dry-out region emerge, and how far does it extend into the reservoir? What is the impact of cold CO_2 injection on the integrity of the caprock/wellbore and surrounding reservoir, and how can this impact be minimized?
- How do thermodynamic processes, such as heat transfer and phase change, affect CO_2 flow behavior during injection into the reservoir and subsequent propagation within the storage formation?

2. Method

2.1. Numerical simulator

The T2WELL-ECO2M simulator (Pan & Oldenburg, 2014; Strpic et al., 2021) has been used for this study because it provides coupled well-reservoir simulation capabilities for CO_2-brine systems over a wide range of *P*-*T* conditions. T2WELL is an extension to TOUGH2, a general-purpose numerical simulation code for non-isothermal flows of multi-component, multiphase fluids in multi-dimensional porous and fractured media (Pruess et al., 2012). T2WELL-ECO2M uses an explicit tabulated file to describe the density, viscosity, and enthalpy of pure CO_2. It allows modifying this file and including a new data set based on a different equation of state (EOS). Compared with the earlier version of T2WELL, where the ECO2N module is applied, ECO2M covers the thermophysical properties of CO_2 in a broader range of temperature (between -18 and 360 °C) and pressure (between 0.001 MPa and 200 MPa). The simulation tool uses Altunin's correlation (1975) to describe the thermophysical properties of CO_2 in its original state. One of the main advantages of ECO2M is its capability to describe all possible phase changes of CO_2 between gaseous, supercritical, and liquid states, which is crucial for studying different operational pressure and temperature conditions.

The other necessary functionality of T2WELL is coupling the wellbore and reservoir by considering two different sub-domains controlled by different underlying flow physics and the ability to solve strongly non-linear and non-isothermal multiphase CO_2 flow equations within the wellbore and storage formation. The multiphase Darcy's law describes three-dimensional flow through the porous media (i.e., reservoir). Viscous flow within the wellbore is modeled by a one-dimensional momentum equation known as the drift flux model (Shi et al., 2005). In addition, brine evaporation and CO_2 solubility are included as analytical functions. The partitioning of H_2O and CO_2 among co-existing aqueous and CO_2-rich phases are derived from the equality of the chemical potential of all components in various phases as a function of pressure, temperature, and salinity. T2WELL-ECO2M utilizes a semi-analytical heat exchange calculation approach to model the heat exchange between wellbore fluid and confining beds and regions outside the flow domain. This approach significantly enhances computational efficiency. Further details of the formulations used in the T2WEll-ECO2M simulator can be found in Pan and Oldenburg 2014. Below we focus on demonstrating the applicability of the code by focusing on the details of the interesting behavior of a model well-reservoir system undergoing CO_2 injection and dry out.

2.2 Conceptual model description

A synthetic two-dimensional radial model of 10 km in radius is considered, schematically shown in Figure 1. The storage reservoir consists of a 20 m thick permeable formation (ϕ = 0.2 and K = 250 mD) with a depth range of 2480 to 2500 meters, overlaid by a 50 m thick cap rock (ϕ = 0.1 and K = 0.01 mD) with the depth range 2430 to 2480 meters. Homogeneous domains are assumed for both the storage formation and cap rock. The ratio of horizontal to vertical permeability is set to 1. The wellbore and porous media are initially filled with water. The water salinity was set to zero to study only the dry-out phenomenon due to evaporation in the well-near reservoir region and to decouple salt precipitation and its potential effects on pore blockage and pressure build-up. The assumed surface conditions of 20 °C and 1 atm, hydrostatic pressure gradient of 10.4 kPa/m, and geothermal gradient of 0.016 °C/m resulted in storage formation pressure and temperature equal to 26 MPa and 60°C, respectively. In the model, the wellbore is situated on the far-left side and extends from the surface down to the reservoir, positioned at a depth of 2500 meters. The internal diameter of the wellbore is 15 cm. The wellbore is solely connected to the storage section located between 2480 and 2500 meters, with no connection assumed along other parts. In these regions, a semi-analytical approach for heat exchange is utilized instead.

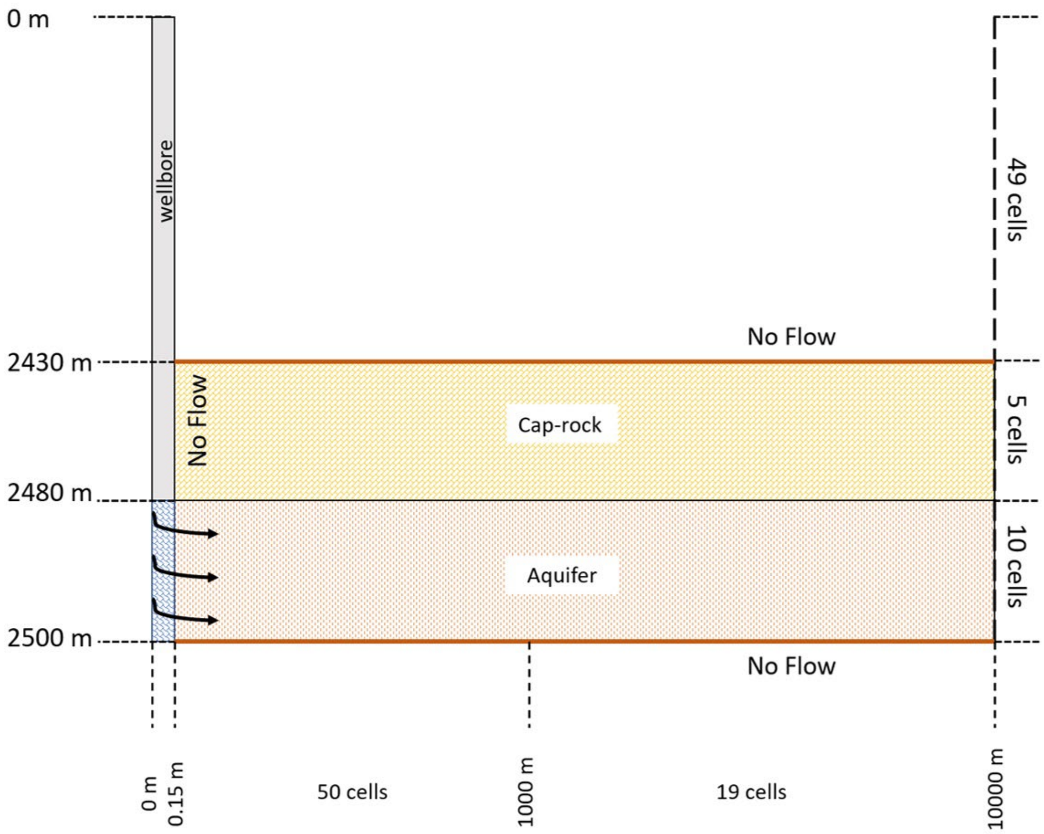

Figure 1: Schematic illustration of the model with the wellbore, storage formation, and cap rock

The wellbore is discretized into 49 grids, each with a uniform length of 50 meters, up to the top of the cap rock at a depth of 2430 meters. Beyond that point, the cap rock section is divided into five layers with thicknesses that vary from 30 meters at the top to 2 meters at the bottom. The storage formation is divided into ten layers, each with a constant thickness of 2 meters. The porous medium is also discretized radially with variable mesh size so that finer mesh is used near the wellbore to capture different phenomena more accurately and gradually becomes coarser towards the outer boundary. The simulation model comprises a total of 1100 cells, including both the reservoir and wellbore. Of these cells, 65 are located within the wellbore, while 690 and 345 are within the reservoir and cap rock sections, respectively.

An infinite volume grid is utilized at the rightmost side of the reservoir and caprock (i.e., the Dirichlet boundary condition) to maintain constant pressure and temperature at the initial reservoir conditions. No-flow boundaries are assumed for the caprock's upper portions and the reservoir's lower portions. The leftmost boundary condition is governed by the injection rate assigned to the topmost cell in the wellbore. Dry CO_2 is injected from the topmost wellbore grid, entering the reservoir along the ten bottommost cells (Figure 1). An extra high-volume cell above the wellhead is considered to maintain the operational condition. The Van Genuchten-Mualem model (Genuchten, 1980; Mualem, 1976) is used for capillary pressure and relative permeability inside the reservoir, and Corey's model for relative permeability inside caprock. Typically, the capillary pressure is more significant in the caprock than in the sandstone reservoir because the cap rock has smaller pore sizes. The parameters of the Van Genuchten model are selected to imitate this phenomenon. Additional information about the conceptual model can be found in Table 1, while capillary pressure and relative permeability curves are depicted in Figure 2.

Formation Properties	**Values**	
	Storage	**Cap rock**

Thickness [m]	20	50
Porosity [-]	0.2	0.1
Permeability [mD]	250	1e-2
Thermal conductivity [W/m.°C]	2.5	1.72
Rock grain Specific Heat [J/Kg °C]	1000	1000
Compressibility [1/Pa]	8.5e-10	8.5e-10
Transport Parameters	**Values**	
	Storage	**Cap rock**
Relative permeability	Van Genuchten model: λ= 0.7, S_{lr} = 0.3, S_{ls} = 0.95, S_{gr} =0.05	Corey's model: S_{lr} = 0.3, S_{gr} = 0.05
Capillary pressure	Van Genuchten model: λ = 0.457, S_{lr} = 0.25, $1/P_0$ = $8*10^{-5}$, P_{max} = 10^7, S_{ls} = 0.999	Van Genuchten model: λ = 0.5, S_{lr} = 0.25, $1/P_0$=10^{-5}, P_{max} = 10^8, S_{ls} = 1
Wellbore Properties	**Values**	
Internal diameter (I.D.) [m]	0.15	
Length [m]	2500	
Injection temperature [°C]	5	
Wellbore roughness [m]	5e-5	
Injection rate [kg/s] @ wellhead	10	
Thermal Conductivity [W/m. °C]	2.5	
General Properties	**Values**	
Temperature gradient [°C/m]	0.016	
Pressure gradient [Pa/m]	1.04e4	
Surface pressure [Pa]	1.01e5	
Surface temperature [°C]	20	

Table 1: Model properties

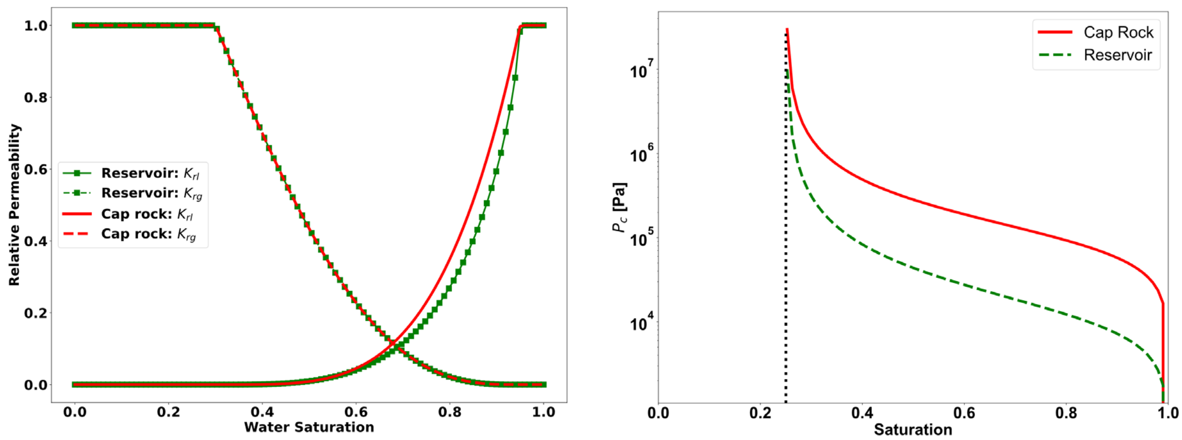

(a) (b)

Figure 2: (a) relative permeability curves and (b) capillary pressure curves used within cap rock and reservoir.

Case description

A synthetic case is utilized to investigate the CO_2 flow inside the wellbore, comprising phase transitions, pressure/temperature profiles, and the resulting CO_2 front, thermal front, and dry-out region within the reservoir. The injection of dry CO_2 at a constant mass flow rate of 10 kg/sec as a boundary condition, a temperature of 5°C, and a pressure of 10.1 MPa right above the wellhead is considered for this purpose. This injection condition results in a liquid CO_2 state above the wellhead. Liquid CO_2 injection is selected for several reasons, including testing the minimum temperature that T2WELL-ECO2M can handle, accounting for phase changes in the wellbore, and potentially offering an energy-efficient injection concept (Vilarrasa et al., 2013). When injection starts, CO_2 flows 2500 meters to reach the bottomhole while experiencing thermal processes such as heat convection, conduction, Joule-Thomson, and frictional flow. As a combined result of these processes, the bottomhole temperature may significantly differ from the initial injecting temperature (i.e., 5 °C) and initial reservoir temperature (i.e., 60 °C), which affect CO_2 propagation within the storage formation.

This study investigates the flow and heat propagation within the reservoir along three lines at distinct depths. The top layer is the first row of cells beneath the interface between the cap rock and storage formation at 2480 meters, while the center layer is in the middle of the reservoir at a depth of 2490 meters. The bottom layer is positioned at the bottommost row of the reservoir at a depth of 2500 meters (Figure 1).

3. Results

3.1. Characterization of CO_2 flow within the wellbore

Figure 3 shows the evolution of CO_2 a) saturation, b) pressure, and c) temperature within the wellbore over the whole simulation time (i.e., two years). The double dashed line represents the front between water that initially filled the wellbore and injected CO_2, and the vertical dashed line reflects the filling time. Filling time refers to the required time for CO_2 to push the water from the wellbore into the reservoir. In these figures, three regions are recognized, summarized as follows: (I) at the initial state (t = 0 sec), the well is filled by water and pressure, and temperature follows the hydrostatic pressure and geothermal gradient along the wellbore. (II) after injection starts, a narrow transition zone can be recognized where the wellbore flow changes into a multiphase where both CO_2 and brine are flowing together. As injection starts, CO_2 saturation within the wellbore increases, displacing the water within the wellbore into the reservoir (Figure 3-a). In this period, according to Figure 3-b, for a short time, ca. 500 seconds (ca. 8.5 mins), the overall pressure profile decreases, and then until the filling time, pressure build-up is observed. It can be attributed to the higher flow resistance within the porous medium compared to the wellbore. The pressure build-up reaches its peak at the time of filling. The whole transient time lasts for 77 minutes. From the practical point of view, before starting the CO_2 injection, water within the wellbore will be replaced by injecting cushion gas to prevent contact of water with CO_2 and possible corrosion within the tubing. However, T2WELL-ECO2M only models CO_2, water, and salt and therefore cannot model this procedure. (III) after filling time, only CO_2 is flowing within the wellbore. Following the filling time, the pressure profile along the wellbore approaches a steady state and remains relatively stable.

Figure 3-c shows the temperature profile evolution over time in the wellbore. Initially, the water temperature in the wellbore follows the assigned geothermal gradient. According to the temperature

gradient, colder water (20 °C) is located at a shallower depth and gradually becomes warmer and reaches 60 °C at the bottomhole. As the injection starts, cold CO_2 at the wellhead pushes the water column within the wellbore into the storage formation. First, the warmer water enters the reservoir, and gradually, colder water from further up in the column enters the reservoir. Due to the high injection rate in the wellbore, the heat transfer mechanism is mainly controlled by convection compared to other mechanisms, such as conduction and frictional effect. The decrease in temperature before the filling time can be captured in Figure 3-c. At the filling time, the CO_2 temperature at the bottomhole is around 40 °C which is significantly higher than the temperature of the injected CO_2 at the surface (5 °C) but still lower than the temperature of the reservoir (60 °C). As illustrated in Figure 3-c, after filling time, even though the temperature at the wellhead reaches the steady state, the temperature at the bottomhole is still changing due to convection heat transfer. As injection continues, colder CO_2 will cool down the surrounding formation, reducing the transfer of heat from the formation to the CO_2 flowing in the wellbore. This leads to the continuous arrival of colder CO_2 to the bottomhole.

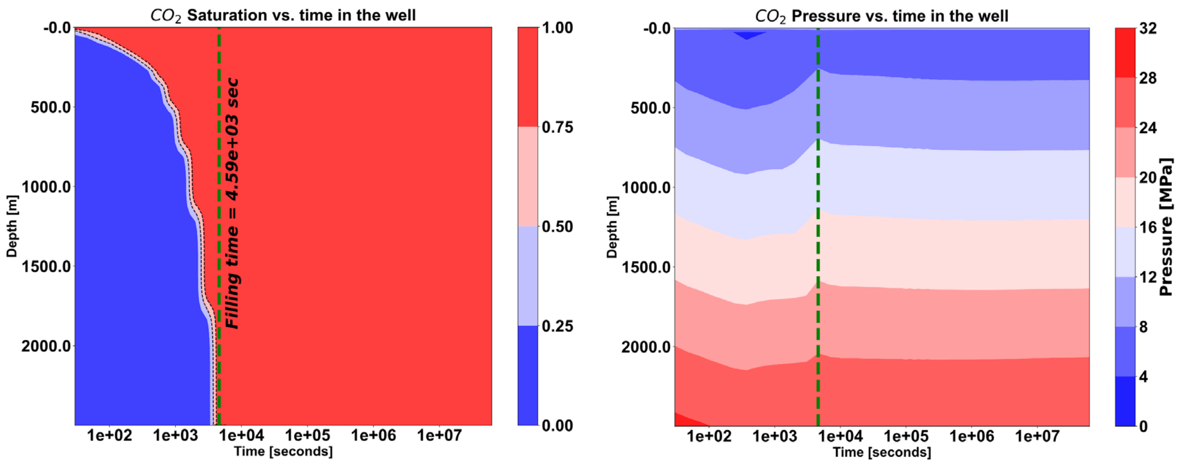

(a) (b)

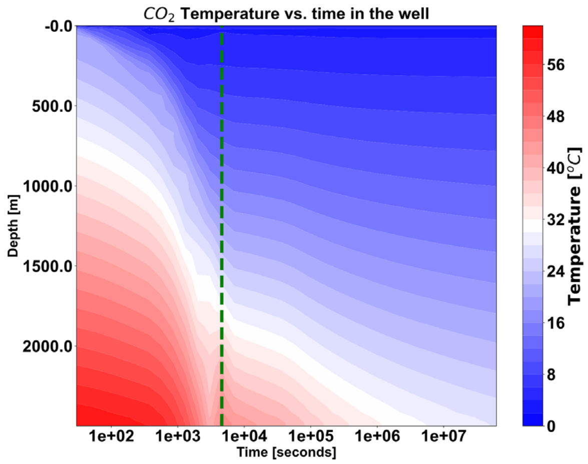

(c)

Figure 3: (a) saturation, (b) pressure, and (c) temperature profiles vs. time within the wellbore

As a complement to Figure 3, we present Figure 4 to illustrate the pressure and temperature profiles along the wellbore at different times. The thick dashed lines correspond to the initially assigned geothermal temperature and hydrostatic pressure. According to Figure 4a-b, it is shown that the pressure profile quickly deviates from the initial hydrostatic pressure, and during the injection, the pressure profile remains constant. It is due to the injection conditions that the CO_2 density becomes large at 940 kg/m^3 which is very close to the original brine density (999 kg/m^3), which was used to calculate the hydrostatic pressure profile (Figure 4-c). Conversely, the temperature profile deviates very slowly from the geothermal gradient, and this is due to an interplay between different heat processes, including convective flow in the wellbore and heat transfer from the ambient formation. The temperature profile clearly illustrates that CO_2 is heating up as it goes down the wellbore but with a slower gradient than the geothermal gradient. Therefore, the temperature at the bottomhole is significantly lower than the reservoir temperature, consistent with field observations reported in numerous articles(Bissell et al., 2011; Lu & Connell, 2014a, 2014b; Paterson et al., 2008, 2010).

In addition, the data in Figure 4a, b can be used for two purposes: (a) To indicate at which depth phase transition can occur and track its development, and (b) to show how fast phase changes arise/diminish, and the pressure and temperature reached at steady-state conditions. In this case, phase transitions can be captured twice: the first is at the early stages, when phase change involves the transition from liquid (at the wellhead) to gaseous state. This phase change happened right after the injection started and gradually expanded within the wellbore. After 244 seconds, the phase-change front expanded up to 300 meters, and after that, the expansion length reduced and completely diminished after 858 seconds. The second transition occurred at a depth of 1750 meters at t = 3019 s, marking the initial point at which CO_2 achieved the conditions for a supercritical state (Figure 4-b). Over approximately 40 days, CO_2 flowed in a supercritical state below a depth of 1750 meters, gradually diminishing until it flowed solely in the liquid state.

Phase transition and CO_2 properties continuously change over the injection period, initially from liquid to gas and later from liquid to supercritical and vice versa. To gain a more comprehensive understanding of the phase transitions and behavior during the injection period, we plotted temperature and pressure profiles on the CO_2 phase transition diagram, as shown in Figure 4-d. It highlights three different times, (I) first, the initial condition as injection starts (Time = 0 s), (II) second, when all of the water in the wellbore is replaced by CO_2, which is stated by the filling time (Time = 4592 s) and (III) third, at the end of the injection after two years. However, the temperature and pressure variation rate after the filling time is significantly reduced compared to the initial transient flow period. Meanwhile, the Pressure-Temperature profile follows the iso-enthalpy lines. This behavior aligns with previous findings in various studies, indicating that pressure and temperature profiles within the wellbore can transiently change during CO_2 injection. (Li et al., 2015; Liu et al., 2015; Lu & Connell, 2008, 2014a, 2014b).

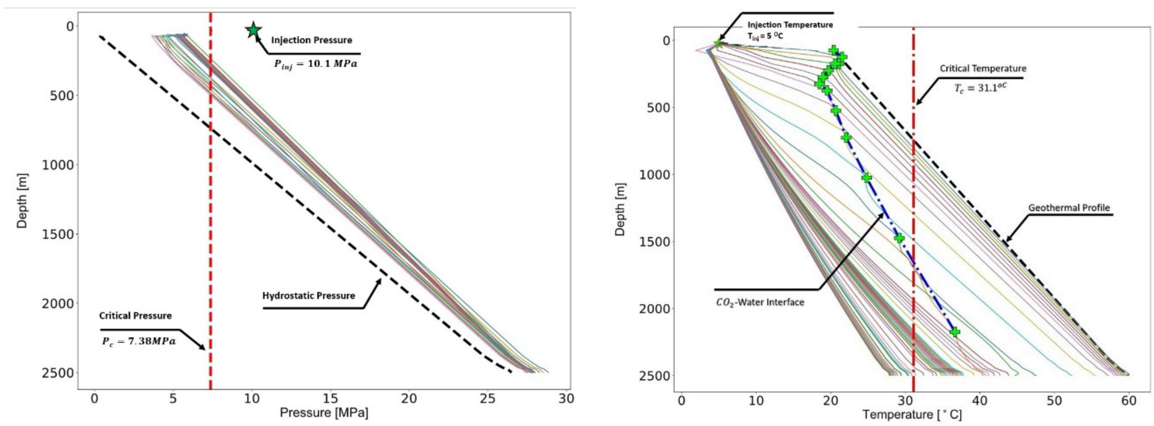

(a) (b)

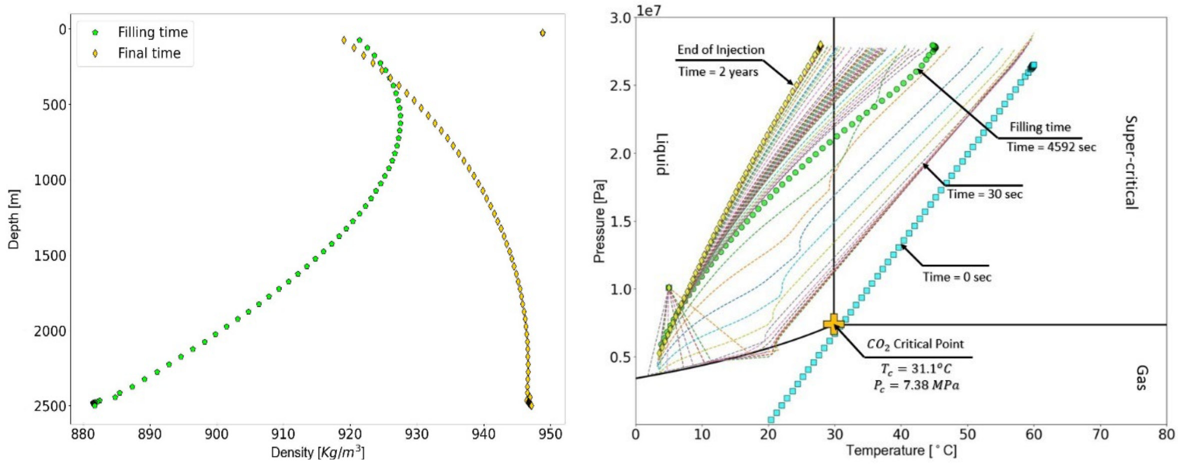

(c) (d)

Figure 4: Pressure and temperature profile evolution along the wellbore: (a) temperature profile vs. depth, (b) pressure profile vs. depth and (c) density profile, and (d) pressure-temperature plot vs. CO_2 phase behavior

Figure 5 illustrates the CO_2 saturation, pressure, and temperature evolution at the wellhead and bottomhole. The CO_2 saturation profile is used to track the location of CO_2 within the wellbore. The temperature profile at the bottomhole is mainly influenced by the colder water in the wellbore before the filling time. As the CO_2 is injected into the reservoir, the colder water is displaced toward the reservoir resulting in a downward trend in the temperature profile. However, just before the filling time, there is a slight uptick in the bottomhole temperature, with a rise of 3 °C from 41 to 44 °C. This increase in temperature can be attributed to the compression of the CO_2 as it enters the storage formation. Following the filling time, a sustained cooling effect is observed, which persists throughout the injection period. This cooling effect is significant, with the bottomhole temperature gradually decreasing to around 30 °C after two years of injection, which is half the actual bottomhole temperature of 60 °C and six times higher than the injection temperature. This continuous cooling can be attributed to the decreasing heat transfer capabilities of the surrounding environment, which reduces its ability to heat the fluid in the wellbore.

In contrast to the bottomhole, the temperature profile at the wellhead displays a distinctly different pattern. Initially, the CO_2 cools down after injection begins, but the temperature remains higher than the injected temperature (5°C) due to heat exchange with the surrounding environment (20°C). The cooling observed downstream is a result of decompression or expansion. The pressure at surface (one cell above wellhead) is maintained at 10.1 MPa to keep the CO_2 in a liquid state, whereas the pressure at the wellhead drops to approximately 5 MPa. This sudden pressure drop causes expansion, leading to a phase transition from liquid to gas and a decrease in temperature due to the Joule-Thomson effect. The cooling effect at the wellhead stabilizes within a few hundred seconds, reaching a steady temperature of around 3.5°C. The combined effect of these heat processes results in a temperature at the wellhead significantly lower than the ambient temperature (20°C) and slightly lower than the injection temperature.

The pressure profile at the bottomhole is mainly governed by the injection rate. In contrast, the pressure value at the wellhead includes the pressure profile within the wellbore and overpressure from the reservoir. As illustrated in Figure 5, the pressure profile at the bottomhole is relatively constant and around 2 MPa higher than reservoir pressure. The pressure profile at the wellhead shows little pressure build-up due to higher resistance toward flow within the reservoir. This variation is limited to the filling time; after that, no pressure change is observed in the wellhead.

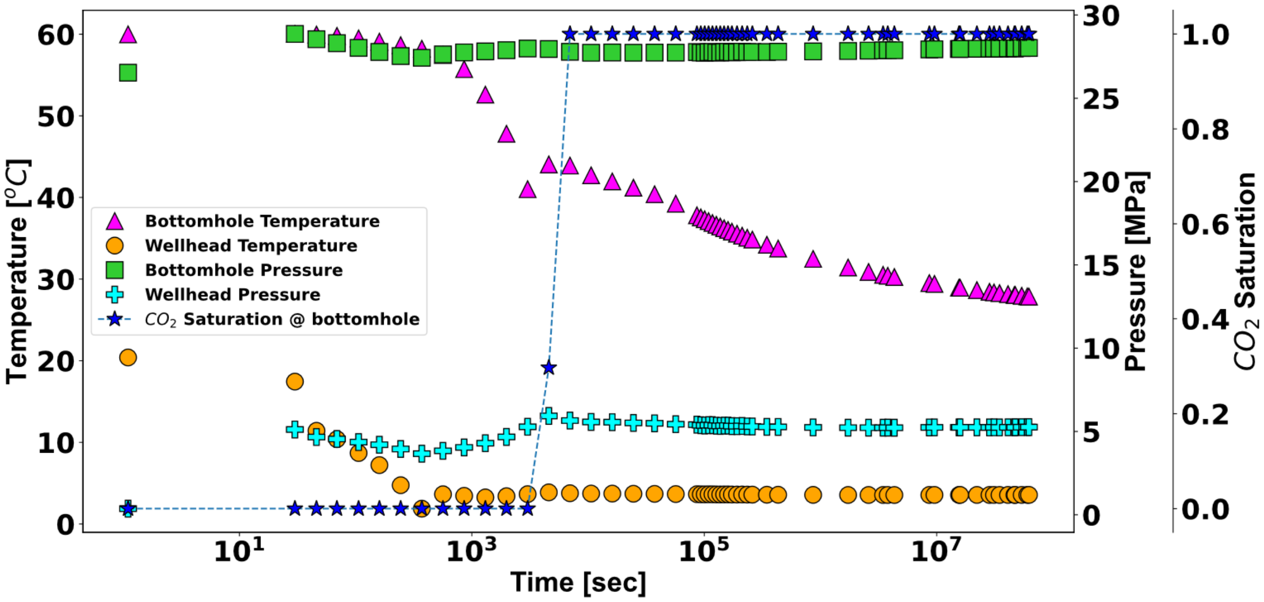

Figure 5: Tracking the pressure, temperature, and saturation profile at the wellhead and bottomhole as a function of time.

3.2. Characterization of CO_2 flow within the storage formation

Monitoring pressure, temperature, and saturation propagation within the reservoir is crucial for practical purposes such as tracking CO_2 plume migration and identifying potential issues related to wellbore and storage integrity. The properties of CO_2 in the wellbore can impact the flow characteristics and features of the reservoir, including heat propagation, the dry-out region near the wellbore, and the movement of CO_2 away from the wellbore. The dynamics of CO_2 plume are primarily governed by the density of CO_2, which in turn is controlled by temperature. Figure 6 depicts the propagation of CO_2 saturation, temperature, and pressures over four different time frames, 100 days, one year, 1.5 years, and two years. The gravity override caused by the difference between CO_2 and water densities is evident in Figure 6 a-d. (Alkan et al., 2023).

As cold CO_2 is injected into the reservoir, it creates a cool zone near the wellbore. However, as it travels deeper into the reservoir, its temperature gradually increases, causing a change in density. The CO_2 density is higher near the wellbore (916 kg/m^3) and lower at the plume front (790 kg/m^3). This change in density causes the CO_2 to migrate preferentially through the upper portion of the reservoir and exhibit a more stable front near the wellbore. Another notable observation is that even though the caprock has considerably lower permeability than the storage formation, the CO_2 still advances slightly into the caprock near the wellbore. This region is of practical importance, as it could potentially result in leakage, and further investigation is necessary.

Temperature propagation is illustrated in Figure 6 e-h, which shows a significantly lower rate of propagation in comparison with CO_2 migration. To better understand the low propagation of heat in comparison with CO_2 saturation, thermal and pressure diffusivity can be compared (Pruess et al., 2012). Thermal diffusivity can be defined by Equation 1, in which λ is thermal conductivity, ρ_r is rock density, and C_r is rock-specific heat. Pressure diffusivity is calculated by Equation 2, in which K is permeability, ϕ is rock porosity, c is fluid compressibility, and μ is the fluid density. The corresponding parameter values are summarized in Table 1, and based on the values, pressure diffusivity is around one [m^2/s] while thermal diffusivity is 10^{-6} [m^2/s], several orders smaller than pressure diffusivity.

$$\Theta = \frac{\lambda}{\rho_r \, C_r} \qquad \text{Equation 1}$$

$$D_p = \frac{K}{\phi c \, \mu} \qquad \text{Equation 2}$$

The cooling of the storage formation is limited to a relatively small area near the wellbore and back of the casing, as Rutqvist (2012) noted. This cooling can cause a significant decrease in temperature, which may alter the stress state and activate new fractures closer to failure conditions. Furthermore, cooling the lower part of the cap rock that is in contact with the storage formation can also activate or destabilize fractures within the cap rock, leading to safety concerns and the risk of leakage (Sagu & Pao, 2013; Vilarrasa & Laloui, 2016). In light of these observations, it is crucial to consider coupled thermal-hydrologic-mechanical (THM) geomechanical simulations when planning CO_2 storage, as this can help identify potential issues with cap rock stability, cap rock leakage, and induced seismicity (Rutqvist, 2012).

Figure 6 i-l illustrates the propagation of pressure waves within storage formation and caprock resulting from CO_2 injection. The pressure distribution follows the expected pattern of higher pressure at the bottom and lower pressure at the top, which also causes lower fluid density at the top and higher density at the bottom. On the other hand, from a geomechanical standpoint, pressure propagation through the cap rock may activate fractures and increase the risk of CO_2 leakage from the storage formation. Therefore, it is crucial to consider the impact of pressure propagation on the caprock stability and potential leakage when planning CO_2 storage.

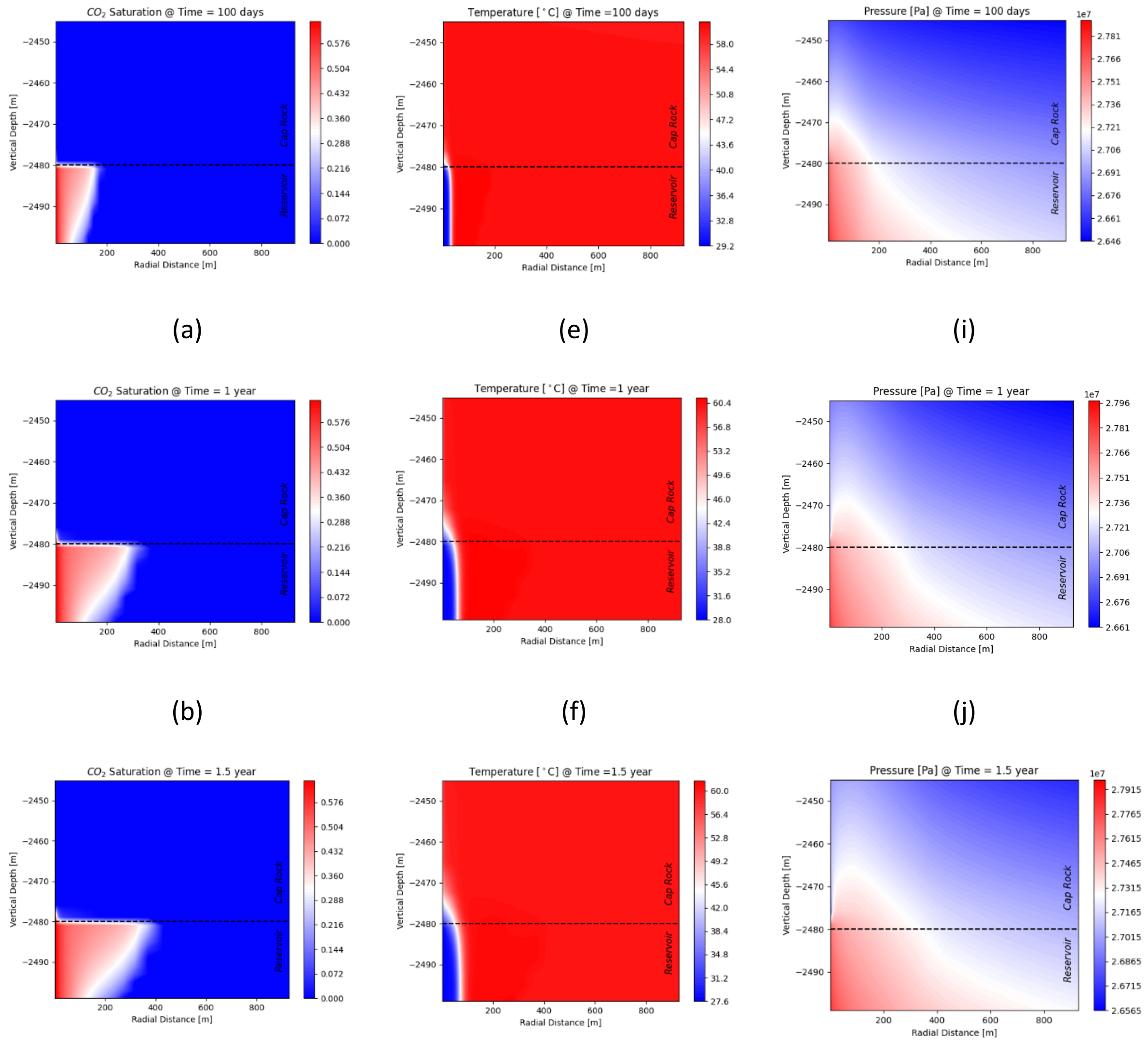

(a) (e) (i)

(b) (f) (j)

(c) (g) (k)

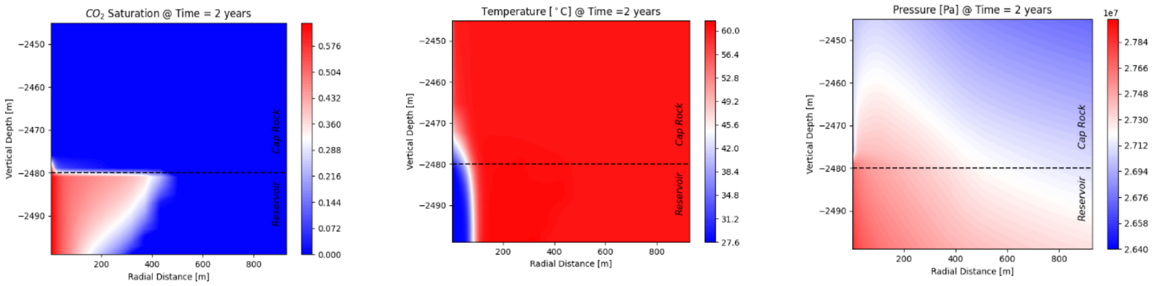

(d) (h) (l)

Figure 6: CO_2 Saturation, temperature, and pressure profiles within cap rock and storage formation at four different times: 100 days, 1, 1.5, and 2 years.

Figure 7 demonstrates the propagation of pressure, temperature, and saturation of both CO_2 and water along the center of the reservoir as a function of distance from the wellbore after two years of injection. To better visualize the profiles near the wellbore, the x-axis is shown on a logarithmic scale. When CO_2 injection reaches the reservoir, a two-phase region forms where the CO_2-rich phase and brine flow together. Behind this front, residual brine will remain trapped and be exposed to dry CO_2, initiating the evaporation regime. As a result, the molar water fraction in the CO_2 stream increases. If the injection continues for a sufficient period, all the remaining water will evaporate and dissolve into dry CO_2, forming a dry-out region.

Figure 7 presents three different fronts, namely the CO_2 front, thermal front, and evaporation front. The CO_2 front is where the CO_2 saturation becomes zero, and water saturation becomes one. The thermal front represents where the reservoir temperature decreases from its initial value. Just ahead of this front, there is a slight increase in temperature due to the exothermic reaction of CO_2 dissolution in water (e.g., up to 5°C). The evaporation front is where all the water in the reservoir is evaporated by dry CO_2, creating a dry-out region. In this zone, the water saturation gradually decreases below the irreducible water saturation and eventually reaches zero, whereas the CO_2 saturation reaches one as no salt is included in this simulation. Along the CO_2 profile, four regions can be identified, which include the dry-out region, the transition region where CO_2 flows at irreducible water saturation and causes continuous evaporation of water, the two-phase region where both CO_2 and brine flow simultaneously, and the single-phase brine flow that occurs far deep in the reservoir where no CO_2 has yet arrived.

The evaporation front is determined by two key parameters: (a) the evaporation onset time and (b) the extent of the dry-out region. Two main factors govern these parameters: i) the migration speed of the dry-out zone, which is influenced by viscous forces such as injection rate and horizontal permeability of the storage formation, and ii) the buoyancy force, which is affected by factors such as CO_2 density, vertical permeability, and the rate of brine counterflow. (Miri & Hellevang, 2016).

The relative migration rates of the various fronts in our simulations are as follows: CO_2 front >> thermal front > evaporation front. The thermal front lags behind the CO_2 front due to the rock heat capacity causing a delay in heat propagation. The evaporation front is much farther behind and may not occur during injection in some cases. Figure 8 illustrates the location of the CO_2 and thermal fronts at different layers within the reservoir over time to highlight the discrepancies between them. The speed of the thermal front is far lower than the CO_2 front, which agrees with the pressure and thermal diffusivity calculation presented earlier and simulation results (Rayward-Smith & Woods, 2011). The migration speed of the fronts also varies at different depths. The migration rate of the CO_2 front is higher in the top layer due to the buoyancy force, while the thermal front propagates slower due to its interaction with the cap rock.

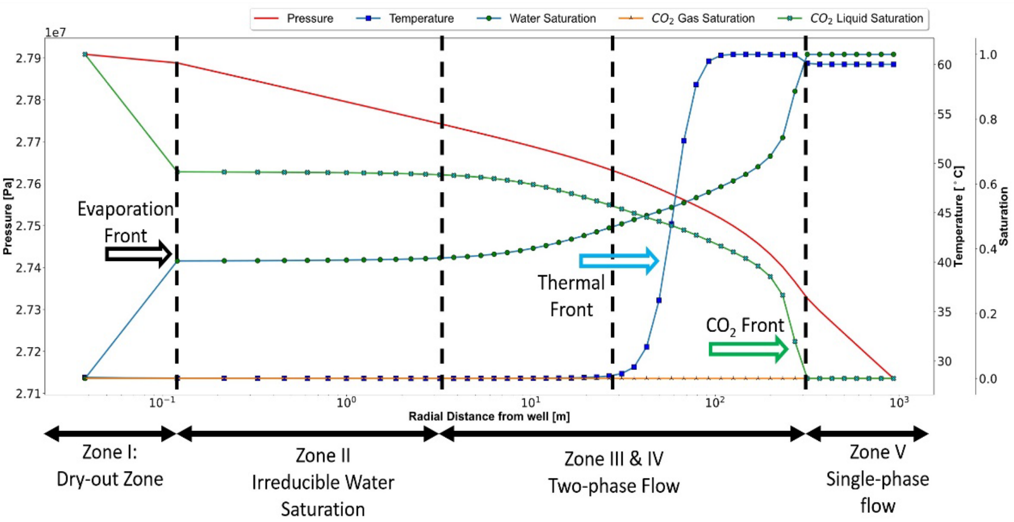

Figure 7: Radial propagation of main reservoir parameters after two years of continuous CO_2 injection

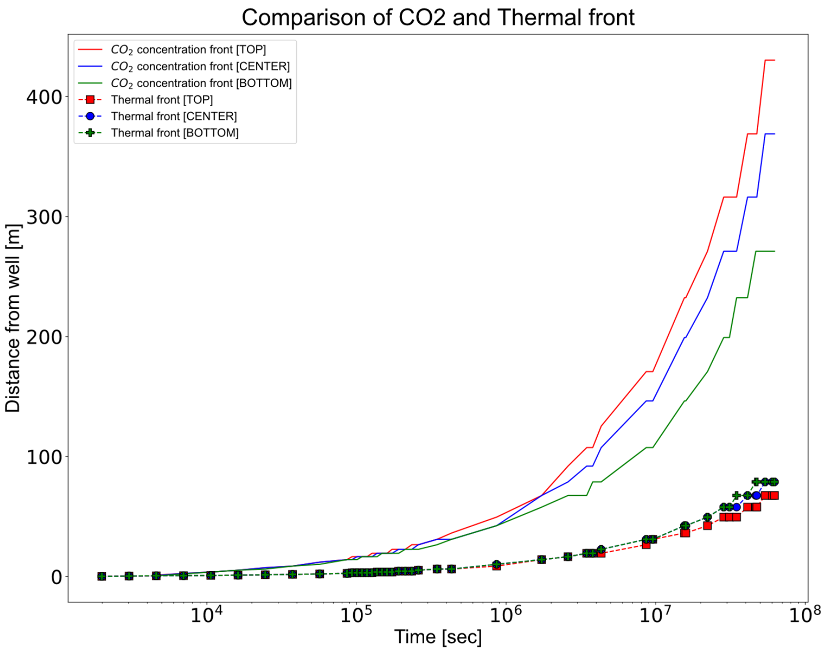

Figure 8: Mapping location of CO_2 front and thermal front as a function of time along layers located at different depth

4. Discussion

Numerical investigations of cold CO_2 injection in a deep aquifer using T2WELL-ECO2M reveal distinct thermal and hydraulic processes. In the wellbore, CO_2 experiences heating due to ambient heat exchange, compression, and frictional loss during its downward flow. However, the heating rate is typically lower than the geothermal gradient, resulting in CO_2 arriving at the bottomhole with a lower temperature (30 °C) than the reservoir temperature (60 °C). Upon entering the reservoir, the colder CO_2 cools down the surrounding rock. Additionally, minor cooling (1-2 °C) can occur due to the Joule-Thomson effect and water vaporization. However, in the aquifer, the Joule-Thomson effect is less pronounced than we expect it to be in depleted hydrocarbon reservoirs. Dissolving CO_2 into brine is exothermic and can raise the temperature by up to 5 °C, consistent with prior simulation findings and field observations. (Bissell et al., 2011; Han et al., 2010; Lu & Connell, 2014b, 2014a; Paterson et al., 2008, 2010).

The reservoir can be divided into five regions around the wellbore based on hydraulic and thermal processes, as shown in Figure 7. Initially, CO_2 dissolves in the reservoir brine at the interface between brine and CO_2 front, resulting in a local temperature increase, pH reduction, and improving injectivity by mineral dissolution, shown by region IV. Once the dissolution process is complete, CO_2 displaces the brine, creating a two-phase region (region III) where both fluids co-flow. When the CO_2 ultimately pushed the brine into the reservoir away from the wellbore, immobile water was left as water films. The extent of this region is controlled by relative permeability and capillary pressure curves. In region II, irreducible water is exposed to dry CO_2, and the vaporization process occurs continuously. After a while, when irreducible water is sufficiently exposed to dry CO_2, the whole water will be vaporized, and a dry-out region will be formed (region I).

In this study, CO_2 phase conditions vary during the injection, leading to a short dry-out region near the wellbore (10 cm) where CO_2 at the bottomhole was in supercritical condition. The extent of this region is highly dependent on various parameters, including reservoir properties, CO_2 injection rate, and phase condition. Preliminary results confirm that the dry-out region only extends a relatively short distance from the wellbore, even over a long injection period.

5. Conclusions

This study demonstrated the capability of T2WELL-ECO2M, a numerical code from the TOUGH family of codes, to accurately model the CO_2 injection process in the wellbore and storage formation. The code successfully captured phase transitions, including gaseous to liquid, liquid to supercritical, and vice versa, which is challenging in numerical simulations. The successful modeling of phase transitions by T2WELL-ECO2M opens up opportunities to study various conditions for CO_2 injection, such as injecting cold CO_2 into the system. The code also simulated thermal processes, such as heat exchange with the ambient, Joule-Thomson effect, water vaporization, CO_2 dissolution in the brine, frictional flow, and convection, providing reliable data.

One advantage of T2WELL is its semi-analytical approach to modeling heat exchange, improving computational efficiency. The study observed minor cooling from the Joule-Thomson effect and CO_2 heating due to dissolution in brine. Water vaporization caused by dry CO_2 exposure was adequately captured, but in this specific study, the dry-out region was relatively small, depending on injection conditions and reservoir properties. These findings lay the foundation for further research on the impact of parameters like reservoir heterogeneity, injection rate, CO_2 condition, and wellbore properties on CO_2 flow, which is essential for proper CCS project design.

However, some limitations of using T2WELL-ECO2M were also encountered. First, assigning proper initial conditions, including pressure and temperature profiles within the wellbore, is crucial for obtaining realistic outcomes. Another perspective is that the code's ability to simulate field operations precisely may be limited from a practical standpoint. For example, injection of a different gas as a cushion gas is typically done before CO_2 injection to prevent corrosion, but T2WELL-ECO2M only allows the simulation of a CO_2-NaCl-water system. Clearly the needs of current applications in the area of detailed design of geologic storage systems for CCS motivate further developments of numerical simulation capabilities.

Acknowledgement

The authors are thankful to Wintershall Dea AG for the possibility to publish this paper. Acknowledgement is given to the CLIMIT DEMO Project, grant no. 621097 “INJECTWELL – Experimental and Numerical Assessments of CO_2 Injectivity and Flow Assurance During Storage in Depleted Hydrocarbon Reservoirs”, a joint industry project, sponsored by the CLIMIT Program (collaboration between Gassnova and the Research Council of Norway) and Wintershall Dea AG.

References

Aakre, H., Mathiesen, V., & Moldestad, B. (2018). Performance of CO2 flooding in a heterogeneous oil reservoir using autonomous inflow control. *Journal of Petroleum Science and Engineering*, *167*, 654–663. https://doi.org/10.1016/J.PETROL.2018.04.008

Alkan, H., Burachok, O., & Kowollik, P. (2023). Geologic carbon storage: key components. *Surface Process, Transportation, and Storage*, 325–422. https://doi.org/10.1016/B978-0-12-823891-2.00009-0

Al-Khdheeawi, E. A., Vialle, S., Barifcani, A., Sarmadivaleh, M., Zhang, Y., & Iglauer, S. (2018). Impact of salinity on CO2 containment security in highly heterogeneous reservoirs. *Greenhouse Gases: Science and Technology*, *8*(1), 93–105. https://doi.org/10.1002/GHG.1723

André, L., Azaroual, M., & Menjoz, A. (2010). Numerical simulations of the thermal impact of supercritical CO2 injection on chemical reactivity in a carbonate saline reservoir. *Transport in Porous Media*, *82*(1), 247–274. https://doi.org/10.1007/S11242-009-9474-2/METRICS

Bissell, R. C., Vasco, D. W., Atbi, M., Hamdani, M., Okwelegbe, M., & Goldwater, M. H. (2011). A full field simulation of the in Salah gas production and CO2 storage project using a coupled geo-mechanical and thermal fluid flow simulator. *Energy Procedia*, *4*, 3290–3297. https://doi.org/10.1016/J.EGYPRO.2011.02.249

Buursink, M. L. (2014). Significance of carbon dioxide density estimates for basin-scale storage resource assessments. *Energy Procedia*, *63*, 5130–5140. https://doi.org/10.1016/J.EGYPRO.2014.11.543

Dalkhaa, C., Jiang, T., Burton-Kelly, M. E., Scharenberg, M., Smith, V., Walker, J. L., Duguid, A., Heinrichs, M. R., Bosshart, N. W., & Sorensen, J. A. (2022). A simulation study of carbon storage with active reservoir management. *Greenhouse Gases: Science and Technology*, *12*(1), 4–23. https://doi.org/10.1002/GHG.2119

Finley, R. J., Frailey, S. M., Leetaru, H. E., Senel, O., Couëslan, M. L., & Marsteller, S. (2013). Early Operational Experience at a One-million Tonne CCS Demonstration Project, Decatur, Illinois, USA. *Energy Procedia*, *37*, 6149–6155. https://doi.org/10.1016/J.EGYPRO.2013.06.544

Genuchten, M. Th. van. (1980). A Closed-form Equation for Predicting the Hydraulic Conductivity of Unsaturated Soils. *Soil Science Society of America Journal*, *44*(5), 892–898. https://doi.org/10.2136/SSSAJ1980.03615995004400050002X

Han, W. S., Stillman, G. A., Lu, M., Lu, C., McPherson, B. J., & Park, E. (2010). Evaluation of potential nonisothermal processes and heat transport during CO2 sequestration. *Journal of Geophysical Research: Solid Earth*, *115*(B7). https://doi.org/10.1029/2009JB006745

Henninges, J., Liebscher, A., Bannach, A., Brandt, W., Hurter, S., Köhler, S., & Möller, F. (2011). P-T-ρ and two-phase fluid conditions with inverted density profile in observation wells at the CO2 storage site at Ketzin (Germany). *Energy Procedia*, *4*, 6085–6090. https://doi.org/10.1016/J.EGYPRO.2011.02.614

Hill, B., Hovorka, S., & Melzer, S. (2013). Geologic Carbon Storage Through Enhanced Oil Recovery. *Energy Procedia*, *37*, 6808–6830. https://doi.org/10.1016/J.EGYPRO.2013.06.614

Hovorka, S. D., Benson, S. M., Doughty, C., Freifeld, B. M., Sakurai, S., Daley, T. M., Kharaka, Y. K., Holtz, M. H., Trautz, R. C., Nance, H. S., Myer, L. R., & Knauss, K. G. (2006). Measuring permanence of CO2 storage in saline formations: the Frio experiment. *Environmental Geosciences*, *13*(2), 105–121. https://doi.org/10.1306/EG.11210505011

Kim, K.-Y., Shik Han, W., Oh, J., Park, E., Lee, P.-K., Kim, K., Oh, J., Lee, P., Han, W. S., & Park, E. (2014). Flow Dynamics of CO 2 /brine at the Interface Between the Storage Formation and Sealing Units in a Multi-layered Model. *Transp Porous Med*, *105*, 611–633. https://doi.org/10.1007/s11242-014-0387-3

Kumar, N., Augusto Sampaio, M., Ojha, K., Hoteit, H., & Mandal, A. (2022). Fundamental aspects, mechanisms and emerging possibilities of CO2 miscible flooding in enhanced oil recovery: A review. *Fuel*, *330*, 125633. https://doi.org/10.1016/J.FUEL.2022.125633

Li, X., Xu, R., Wei, L., & Jiang, P. (2015). Modeling of wellbore dynamics of a CO2 injector during transient well shut-in and start-up operations. *International Journal of Greenhouse Gas Control*, *42*, 602–614. https://doi.org/10.1016/J.IJGGC.2015.09.016

Lindeberg, E. (2011). Modelling pressure and temperature profile in a CO2 injection well. *Energy Procedia*, *4*, 3935–3941. https://doi.org/10.1016/J.EGYPRO.2011.02.332

Litynski, J., Rodosta, T., Vikara, D., & Srivastava, R. (2013). U.S. DOE's R&D Program to Develop Infrastructure for Carbon Storage: Overview of the Regional Carbon Sequestration Partnerships and other R&D Field Projects. *Energy Procedia*, *37*, 6527–6543. https://doi.org/10.1016/J.EGYPRO.2013.06.584

Liu, D., Li, Y., Song, S., & Agarwal, R. (2016). Simulation and analysis of lithology heterogeneity on CO2 geological sequestration in deep saline aquifer: a case study of the Ordos Basin. *Environmental Earth Sciences*, *75*(11), 1–13. https://doi.org/10.1007/S12665-016-5754-7/FIGURES/15

Liu, D., Li, Y., Xu, L., & Yu, Y. (2015). Numerical investigation of the influence of interaction between wellbore flow and lateral reservoir flow on CO2 geological sequestration. *Environmental Earth Sciences*, *74*(1), 715–726. https://doi.org/10.1007/S12665-015-4076-5/FIGURES/11

Lu, M., & Connell, L. D. (2008). Non-isothermal flow of carbon dioxide in injection wells during geological storage. *International Journal of Greenhouse Gas Control*, *2*(2), 248–258. https://doi.org/10.1016/S1750-5836(07)00114-4

Lu, M., & Connell, L. D. (2014a). The transient behaviour of CO2 flow with phase transition in injection wells during geological storage - Application to a case study. *Journal of Petroleum Science and Engineering*, *124*, 7–18. https://doi.org/10.1016/J.PETROL.2014.09.024

Lu, M., & Connell, L. D. (2014b). Transient, thermal wellbore flow of multispecies carbon dioxide mixtures with phase transition during geological storage. *International Journal of Multiphase Flow*, *63*, 82–92. https://doi.org/10.1016/J.IJMULTIPHASEFLOW.2014.04.002

Mathieson, A., Midgely, J., Wright, I., Saoula, N., & Ringrose, P. (2011). In Salah CO2 Storage JIP: CO2 sequestration monitoring and verification technologies applied at Krechba, Algeria. *Energy Procedia*, *4*, 3596–3603. https://doi.org/10.1016/J.EGYPRO.2011.02.289

Miri, R., & Hellevang, H. (2016). Salt precipitation during CO2 storage—A review. *International Journal of Greenhouse Gas Control*, *51*, 136–147. https://doi.org/10.1016/J.IJGGC.2016.05.015

Movahedzadeh, Z., Shokri, A. R., Chalaturnyk, R., Nickel, E., & Sacuta, N. (2021). Measurement, monitoring, verification and modelling at the Aquistore CO2 storage site. *First Break*, *39*(2), 69–75. https://doi.org/10.3997/1365-2397.FB2021013/CITE/REFWORKS

Mualem, Y. (1976). A new model for predicting the hydraulic conductivity of unsaturated porous media. *Water Resources Research*, *12*(3), 513–522. https://doi.org/10.1029/WR012I003P00513

Page, B., Turan, G., Zapantis, A., Burrows, J., Consoli, C., Erikson, J., Havercroft, I., Kearns, D., Liu, H., Rassool, D., Tamme, E., Temple-Smith, L., Townsend, A., & Zhang, T. (2020). *The Global Status of CCS 2020: Vital to Achieve Net Zero*. https://www.h2knowledgecentre.com/content/researchpaper1679

Pan, L., & Oldenburg, C. M. (2014). T2Well—An integrated wellbore–reservoir simulator. *Computers & Geosciences*, *65*, 46–55. https://doi.org/10.1016/J.CAGEO.2013.06.005

Pan, L., Oldenburg, C. M., Pruess, K., & Wu, Y.-S. (2011). Modeling and Analysis Transient CO 2 leakage and injection in wellbore-reservoir systems for geologic carbon sequestration †. *Ltd | Greenhouse Gas Sci Technol*, *1*, 335–350. https://doi.org/10.1002/ghg

Paterson, L., Ennis-King, J., & Sharma, S. (2010). Observations of Thermal and Pressure Transients in Carbon Dioxide Wells. *Proceedings - SPE Annual Technical Conference and Exhibition*, *5*, 3449–3460. https://doi.org/10.2118/134881-MS

Paterson, L., Lu, M., Connell, L. D., & Ennis-King, J. (2008). Numerical Modeling of Pressure and Temperature Profiles Including Phase Transitions in Carbon Dioxide Wells. *Proceedings - SPE Annual Technical Conference and Exhibition*, *4*, 2693–2703. https://doi.org/10.2118/115946-MS

Piao, J., Han, W. S., Choung, S., & Kim, K. Y. (2018). Dynamic Behavior of CO2 in a Wellbore and Storage Formation: Wellbore-Coupled and Salt-Precipitation Processes during Geologic CO2 Sequestration. *Geofluids*, *2018*. https://doi.org/10.1155/2018/1789278

Preston, C., Monea, M., Jazrawi, W., Brown, K., Whittaker, S., White, D., Law, D., Chalaturnyk, R., & Rostron, B. (2005). IEA GHG Weyburn CO2 monitoring and storage project. *Fuel Processing Technology*, *86*(14–15), 1547–1568. https://doi.org/10.1016/J.FUPROC.2005.01.019

Pruess, K., Oldenburg, C., & Moridis, G. (2012). *TOUGH2 USER'S GUIDE, VERSION 2*.

Rangriz Shokri, A., Talman, S., Chalaturnyk, R. J., & Nickel, E. (2021). *On the Temporal Evolution of Non-Isothermal Injectivity Behaviour at an Active CO2 Injection Site*. OnePetro. https://dx.doi.org/

Rayward-Smith, W. J., & Woods, A. W. (2011). Some implications of cold CO2 injection into deep saline aquifers. *Geophysical Research Letters*, *38*(6), 6407. https://doi.org/10.1029/2010GL046412

Rutqvist, J. (2012). The geomechanics of CO 2 storage in deep sedimentary formations. *Geotechnical and Geological Engineering*, *30*(3), 525–551. https://doi.org/10.1007/S10706-011-9491-0/FIGURES/4

Sagu, O. L., & Pao, W. K. S. (2013). In-situ stress perturbation due to temperature around borehole during carbon injection. *Asian Journal of Applied Sciences*, *6*(1), 40–49. https://doi.org/10.3923/AJAPS.2013.40.49

Sato, K., Mito, S., Horie, T., Ohkuma, H., Saito, H., Watanabe, J., & Yoshimura, T. (2011). Monitoring and simulation studies for assessing macro- and meso-scale migration of CO2 sequestered in an onshore aquifer: Experiences from the Nagaoka pilot site, Japan. *International Journal of Greenhouse Gas Control*, *5*(1), 125–137. https://doi.org/10.1016/J.IJGGC.2010.03.003

Shi, H., Holmes, J. A., Durlofsky, L. J., Aziz, K., Diaz Teran Ortegon, L. R., Alkaya, B., & Oddie, G. (2005). Drift-Flux Modeling of Two-Phase Flow in Wellbores. *SPE Journal*, *10*(01), 24–33. https://doi.org/10.2118/84228-PA

Sokama-Neuyam, Y. A., Adu-Boahene, F., Boakye, P., Aggrey, W. N., & Ursin, J. R. (2020). Theoretical modeling of the effect of temperature on CO2 injectivity in deep saline formations. *Greenhouse Gases: Science and Technology*, *10*(1), 4–14. https://doi.org/10.1002/GHG.1951

Sokama-Neuyam, Y. A., Aggrey, W. N., Boakye, P., Sarkodie, K., Oduro-Kwarteng, S., & Ursin, J. R. (2022). The effect of temperature on CO2 injectivity in sandstone reservoirs. *Scientific African*, *15*. https://doi.org/10.1016/J.SCIAF.2021.E01066

Strpic, K., Bonduà, S., Bortolotti, V., Macini, P., Battistelli, A., & Pan, L. (2021). *Evaluation of Time-Convolution Approach for Modelling Heat Exchange Between Wellbore and Formation During Multiphase CO2 Injection with T2Well-ECO2M*. OnePetro.

Torp, T. A., & Gale, J. (2004). Demonstrating storage of CO2 in geological reservoirs: The Sleipner and SACS projects. *Energy*, *29*(9–10), 1361–1369. https://doi.org/10.1016/J.ENERGY.2004.03.104

Vilarrasa, V., & Laloui, L. (2016). Impacts of Thermally Induced Stresses on Fracture Stability During Geological Storage of CO2. *Energy Procedia*, *86*, 411–419. https://doi.org/10.1016/J.EGYPRO.2016.01.042

Vilarrasa, V., & Rutqvist, J. (2017). Thermal effects on geologic carbon storage. *Earth-Science Reviews*, *165*, 245–256. https://doi.org/10.1016/J.EARSCIREV.2016.12.011

Vilarrasa, V., Silva, O., Carrera, J., & Olivella, S. (2013). Liquid CO2 injection for geological storage in deep saline aquifers. *International Journal of Greenhouse Gas Control*, *14*, 84–96. https://doi.org/10.1016/J.IJGGC.2013.01.015

Würdemann, H., Möller, F., Kühn, M., Heidug, W., Christensen, N. P., Borm, G., & Schilling, F. R. (2010). CO2SINK—From site characterisation and risk assessment to monitoring and verification: One year of operational experience with the field laboratory for CO2 storage at Ketzin, Germany. *International Journal of Greenhouse Gas Control*, *4*(6), 938–951. https://doi.org/10.1016/J.IJGGC.2010.08.010